1 Gbps Directed Optical Decoder Based on Two Cascaded Microring Resonators

Qiaoshan Chen, **Fanfan Zhang**, **Lei Zhang**, **Yonghui Tian**,
Ping Zhou, **Jianfeng Ding**, **and Lin Yang**
State Key Laboratory on Integrated Optoelectronics
Institute of Semiconductors, Chinese Academy of Sciences, China

Abstract— We report an electro-optic directed optical decoder based on two cascaded microring resonators. PN junctions embedded around the MRRs are employed to modulate the MRRs through the carrier-injection scheme. The optical decoding function from a 2-bit electrical signal to a 4-bit optical signal at the speed of 1 Gbps is performed successfully by the device.

1. INTRODUCTION

Optical directed logic is a paradigm which employs the optical switch network to perform the logical operation [1, 2]. The status of each optical switch in the network is determined by an electrical Boolean signal applied to it. The operation of each optical switch is independent of the operations of other optical switches in the network and the operation result propagates in the network at the speed of light. The overall latency of the optical directed logic circuit is very small and all optical switches perform their operations almost simultaneously [3, 4]. Therefore, the optical directed logic has a very high operation speed and low latency [1–4]. Silicon microring resonator is an attractive structure owing to its outstanding performances, such as compact size, ultra-low power consumption and CMOS-compatible fabrication process. Therefore, the optical directed logic based on silicon microring switches is easy to realize large-scale integration and low-cost manufacture in a high-volume CMOS photonics foundry. A series of optical directed logic circuits have been proposed and even demonstrated [5–9].

We have demonstrated a directed optical decoder [6], whose speed is 10 kbps due to the thermo-optic modulation scheme. In this letter, a directed optical decoder modulated by electric-field-induced carrier injection in forward biased PN junctions is demonstrated, which can perform the decoding function from a 2-bit electrical signal to a 4-bit optical signal at the speed of 1 Gbps.

2. DESIGN AND FABRICATION

The architecture of the directed optical decoder is schematically shown in Fig. 1, which consists of two cascaded electrically modulated add-drop MRRs and three waveguides. Monochromatic continuous light with the working wavelength λ_{work} is coupled into the device through its input port, and modulated by two electrical pulse sequences applied to the MRRs through electric-field-induced carrier injection in forward biased PN junctions.

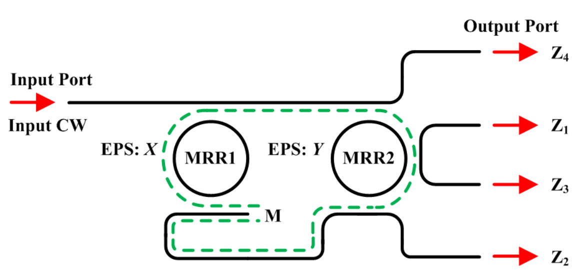

Figure 1: Schematic of the optical device. CW: continuous wave, EPS: electrical pulse signal, MRR: microring resonator.

Each MRR acts as an optical switch and two electrical signals X and Y are used to control the resonance states of two MRRs, respectively. In the previous work [11], thermo-optic effect is employed to tune the resonance state of each MRR and the MRR is on-resonance when the applied voltage is at the high level. In this work, free-carrier dispersion effect is employed to tune the resonance state of each MRR. When carriers are injected into the MRR, the refractive index of the ring waveguide is reduced and its propagation loss is increased simultaneously. In order to achieve high contrast between optical logic 1 and 0, two MRRs are on-resonance at the working wavelength λ_{work} when the applied electrical signals are at the low level and off-resonance at the working wavelength λ_{work} when the applied electrical signals are at the high level. The high and low levels of the optical power at four output ports represent the operation result of logic 1 and 0, respectively. According to the definition above, the electrical logics applied to two MRRs, the states of two MRRs and the operation results at four output ports are summarized in Table 1. Clearly, the architecture in Fig. 1 can perform the decoding function from a 2-bit electrical signal to a 4-bit optical signal.

Table 1: Principle of the directed optical decoder.

Electrical logic of MRR1	Electrical logic of MRR2	Resonance state of MRR1	Resonance state of MRR2	Z_1	Z_2	Z_3	Z_4
0	0	ON	ON	1	0	0	0
0	1	ON	OFF	0	1	0	0
1	0	OFF	ON	0	0	1	0
1	1	OFF	OFF	0	0	0	1

In Fig. 2, the waveguides are sheltered by aluminum trances and pads. The dash lines show where the waveguides are and the green arrows represent the input and output ports of the device.

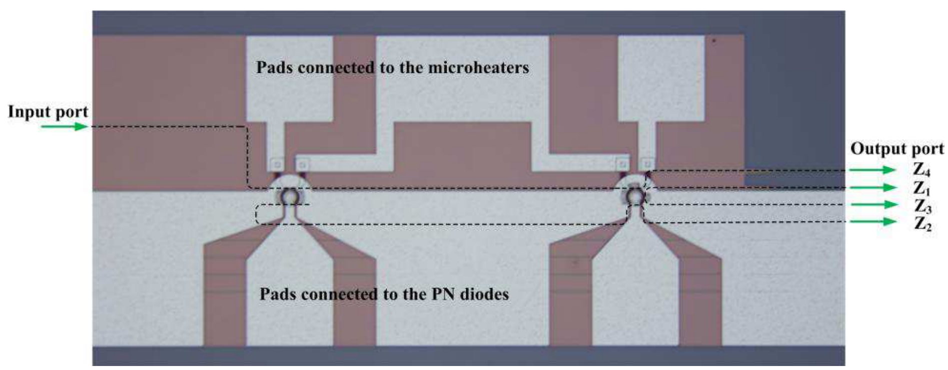

Figure 2: Micrograph of electro-optic directed optical decoder.

3. ANALYSIS OF THE STATIC RESPONSE SPECTRA

In order to determine the working wavelength of the device and the driving voltages of two MRRs, the static response spectra of the device are measured with an amplified spontaneous emission (ASE) source, an optical spectrum analyzer (OSA) and three tunable voltage sources. The light from the ASE source is coupled into the input port of the device through a lensed fiber. The light from the output port of the device is coupled into another lensed fiber and then fed into the OSA. One tunable voltage source is used to tune the microheater of the MRR with shorter initial resonance wavelength, so that its resonance wavelength matches with that of the other MRR. The left two tunable voltage sources are employed to inject carriers into the two PN diodes, respectively. With the applied voltage on the PN diode increasing, the effective refractive index decreases and the resonance wavelength of the MRR moves to the shorter wavelength.

Although two MRRs are designed to have the same structural parameters, they have slightly different initial resonance wavelengths due to the limited manufacturing accuracy. Without any tunable voltage sources applied to the device, the static response spectra at the output ports Z_1–Z_4 are shown in Fig. 3. We can see two dips at 1551.768 nm and 1552.472 nm in the static response spectra at the output port Z_4 (Fig. 3(d)), which are caused by the resonances of MRR2 and MRR1, respectively. MRR2 has three coupling regions while MRR1 has two coupling regions. Except for this, MRR2 has the same structural parameters with MRR1 does. Therefore, MRR2 has a larger optical loss than MRR1 does and the calculated Q factor from the static response spectra is 17642 for MRR1 and 11410 for MRR2. MRR1 has an extinction ratio of 20.4 dB and MRR2 has an extinction ratio of 14.8 dB, because MRR1 is much closer to the critical coupling than MRR2 does in the adopted structural parameters.

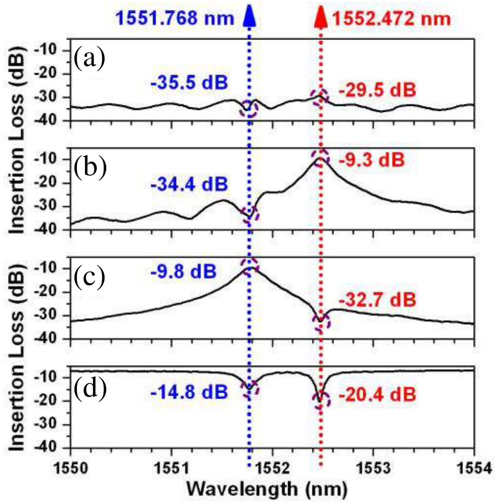

Figure 3: Static response spectra at the output ports (a) Z_1, (b) Z_2, (c) Z_3, and (d) Z_4 without electrical compensating voltage applied to the device.

1552.472 nm is chosen as the working wavelength λ_{work} to achieve a relatively large extinction ratio. When MRR2 is heat up, the effective refractive index of the Si waveguide increases and the resonance wavelength of MRR2 shifts to the longer wavelength. With the voltage applied to the microheater of MRR2 being 2.1 V (the compensating voltage), the resonance wavelength of MRR2 is at the working wavelength. The static response spectra at four output ports Z_1–Z_4 with the compensating voltage are shown in Figs. 4(a), 5(a), 6(a) and 7(a).

Noted that some ripples are observed in the static response spectra at the output ports Z_1 and Z_2, (Figs. 3(a) and 3(b)) due to the interference effect caused by the closed cavity formed by two cascaded MRRs and the facet of port M, as shown in the green dash line in Fig. 1.

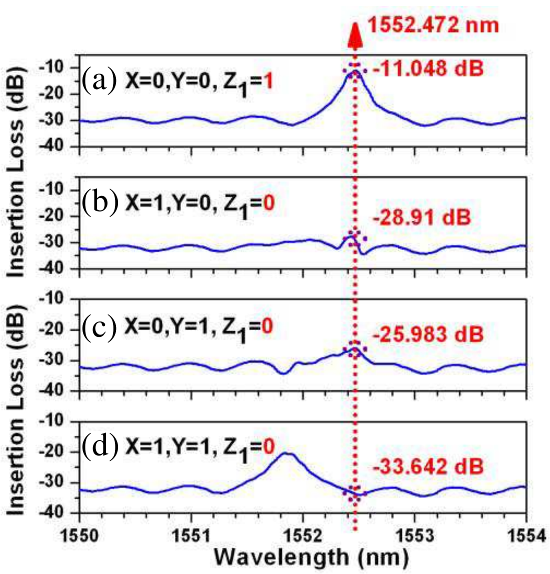

Figure 4: Static response spectra at the output port Z_1 with the voltages applied to the PN junctions of MRR1 and MRR2 being (a) 0 V and 0 V, (b) 1.5 V and 0 V, (c) V and 1.4 V, (d)1.5 V and 1.4 V.

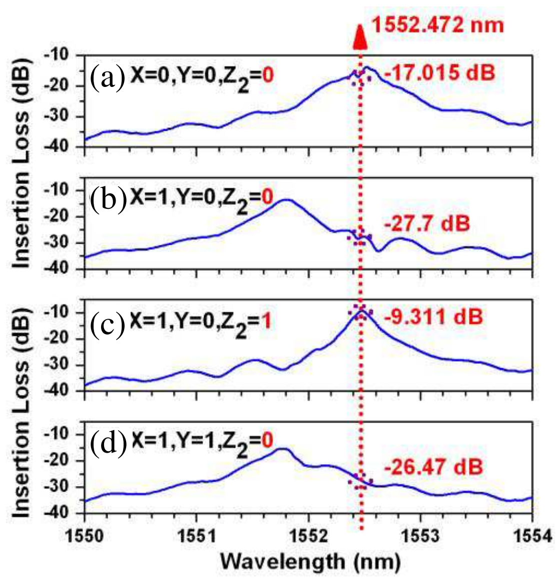

Figure 5: Static response spectra at the output port Z_2 with the voltages applied to the PN junctions of MRR1 and MRR2 being (a) 0 V and 0 V, (b) 1.5 V and 0 V, (c) 0 V and 1.4 V, (d)1.5 V and 1.4 V.

The static response spectra at the output port Z_1 show the drop filtering characteristics of MRR1 and MRR2 (Fig. 4). According to the principle aforementioned, there is a peak when both

MRR1 and MRR2 are on-resonance at the working wavelength (Fig. 4(a)), the optical power at the output port Z_1 is at the high level (representing 1). In other three working statuses, the optical power at the output port Z_1 is at the low level (Figs. 4(b)–(d)).

The static response spectra at the output port Z_2 show the drop filtering characteristics of MRR1 and the through filtering characteristics of MRR2 (Fig. 5). The optical power at the output port Z_2 is at the high level when MRR1 is on-resonance and MRR2 is off-resonance (Fig. 5(c)). In other three working statuses, the optical power at the output port Z_2 is at the low level (Figs. 5(a), 5(b) and 5(d)).

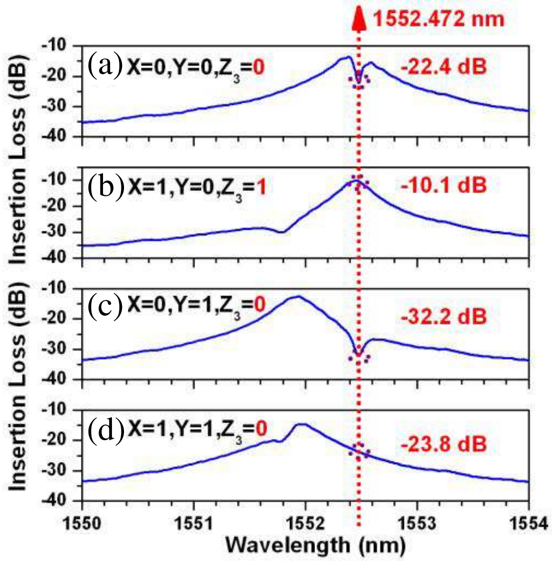

Figure 6: Static response spectra at the output ports Z_3 with the voltages applied to the PN junctions of MRR1 and MRR2 being (a) 0 V and 0 V, (b) 1.5 V and 0 V, (c) 0 V and 1.4 V, (d) 1.5 V and 1.4 V.

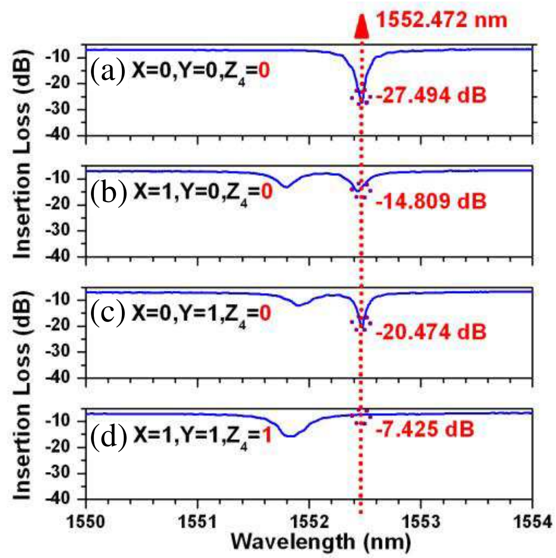

Figure 7: Static response spectra at the output ports Z_4 with the voltages applied to the PN junctions of MRR1 and MRR2 being (a) 0 V and 0 V, (b) 1.5 V and 0 V, (c) 0 V and 1.4 V, (d) 1.5 V and 1.4 V.

The static response spectra at the output port Z_3 show the through filtering characteristics of MRR1 and the drop filtering characteristics of MRR2 (Fig. 6). MRR2 has a much larger full width at half maximum (FWHM) than MRR1 does. So there is a dip in the drop filtering spectra, which can be noticed in Fig. 6(a). The optical power at the output port Z_3 is at the high level when MRR1 is off-resonance and MRR2 is on-resonance (Fig. 6(b)). In other three working statuses, the optical power at the output port Z_3 is at the low level (Figs. 6(b)–(d)).

The static response spectra at the output port Z_4 show the through filtering characteristics of MRR1 and MRR2 (Fig. 7). According to the principle aforementioned, there is a dip when both MRR1 and MRR2 are on-resonance at the working wavelength (Fig. 7(a)), the optical power is at the low level (representing 0). With only the voltage of 1.5 V applied to the PN diode of MRR1, the resonance wavelength of MRR1 shifts to the shorter wavelength (Fig. 7(b)) and the optical power is still at the low level (representing 0). With only the voltage of 1.4 V applied to the PN diode of MRR2, the resonance wavelength of MRR2 shifts to the shorter wavelength (Fig. 7(c)) and the optical power is at the low level (representing 0). The optical power at the output port Z_4 is at the high level when both MRR1 and MRR2 are off-resonance (Fig. 7(d)).

All four static response spectra at four output ports of the device are analyzed above. The results indicate that the device can implement the decoding function from a 2-bit electrical signal to a 4-bit optical signal correctly.

4. DYNAMIC EXPERIMENTAL RESULTS

A monochromatic light with the working wavelength of 1552.472 nm is coupled into a polarization rotator and the light with the TE polarization is coupled into the device by a lensed fiber. Two non-return-to-zero electrical signals with the period of 8 bits generated by two pulse pattern generators are used to modulate the PN diodes of MRR1 and MRR2, respectively. The electrical signals applied to the MRRs have the amplitude of 0.8 V with the offset of 1.1 V. The light at the output ports Z_1–Z_4 are fed into a wideband sampling oscilloscope (Agilent DCA-X 860100D) with an optical head for waveform observation.

The dynamic response of the device at the speed of 1 Gbps is characterized. The results are shown in Fig. 8, in which three periods (i.e., 24 bits) are shown for the input electrical signals and the output optical signals. We have measured those signals one by one and then aligned them with each other in the time axis. The device performs the decoding function from a 2-bit electrical signal to a 4-bit optical signal at the speed of 1 Gbps correctly. There are several positive spikes between two continuous outputs of '0s' at the output port Z_4, which are also observed and have been well explained in the previous work [6]. Note that the power level is same for logical '1' but different for logical '0' in different working statuses at the output ports Z_2 and Z_4, which mainly results from the different extinction ratios of the dips in different working statuses. These phenomena are also observed in the static response spectra (Figs. 5 and 7), where the insertion losses for logical '0' is −17.015, −26.47 and −27.7 dB at the output port Z_2 in different cases respectively, and the insertion losses for logical '0' is −14.809, −20.474 and −27.494 dB at the output port Z_4 in different working statuses respectively.

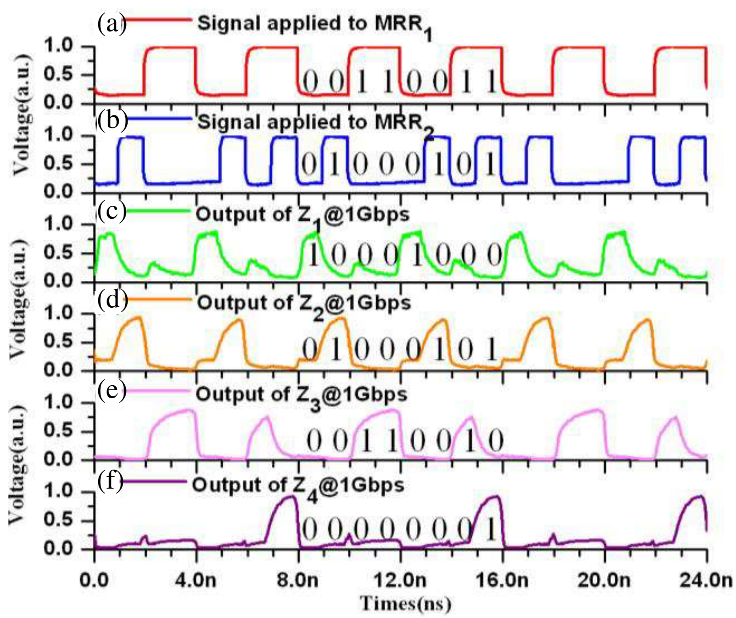

Figure 8: Dynamic operation results of the device at the speed of 1 Gbps. (a) and (b) 1 Gbps electrical signals applied to MRR1 and MRR2, respectively. 1 Gbps decoder operation results at the ports (c) Z_1, (d) Z_2, (e) Z_3, (f) Z_4 respectively.

5. CONCLUSION

In conclusion, we fabricated an electro-optic directed optical decoder based on two cascaded microring resonators. PN junctions embedded around the MRRs are employed to modulate the MRRs through the carrier-injection scheme. The optical decoding function from a 2-bit electrical signal to a 4-bit optical signal at the speed of 1 Gbps is performed successfully by the device.

ACKNOWLEDGMENT

The authors thank Dr. M. B. Yu of IME for device fabrication. This work has been supported by the National Natural Science Foundation of China under grants 61204061, 61235001, and 61377067, by the National High Technology Research and Development Program of China under grants 2012AA012202 and 2013AA014203 and by Scientific and Technological Innovation Cross Team of Chinese Academy of Sciences.

REFERENCES

1. Hardy, J. and J. Shamir, "Optics inspired logic architecture," *Optics Express*, Vol. 15, No. 1, 150–165, 2007.

2. Shamir, J., "Energy efficient computing exploiting the properties of light," *SPIE Optical Engineering+ Applications. International Society for Optics and Photonics*, 88330J-88330J-9, 2013.
3. Caulfield, H. J. and S. Dolev, "Why future supercomputing requires optics," *Nature Photonics*, Vol. 4, No. 5, 261–263, 2010.
4. Caulfield, H. J., R. A. Soref, and C. S. Vikram, "Universal reconfigurable optical logic with silicon-on-insulator resonant structures," *Photonics and Nanostructures-Fundamentals and Applications*, Vol. 5, No. 1, 14–20, 2007.
5. Xu, Q. and R. Soref, "Reconfigurable optical directed-logic circuits using microresonator-based optical switches," *Opt Express*, Vol. 19, No. 9, 5244, 2011.
6. Tian, Y., L. Zhang, R. Ji, et al., "Demonstration of a directed optical decoder using two cascaded micoring resonantors," *Opt. Lett.*, Vol. 36, No. 17, 3314, 2011.
7. Tian, Y., L. Zhang, R. Ji, Lin, Yang, P. Zhou, H. Chen, J. Ding, W. Zhu, Y. Lu, L. Jia, Q. Fang, and M. Yu, "Proof of concept of directed OR/NOR and AND/NAND logic circuit consisting of two parallel microring resonators," *Opt. Lett.*, Vol. 36, No. 9, 1650, 2011.
8. Zhang, L., R. Ji, Y. Tian, L. Yang, P. Zhou, Y. Lu, W. Zhu, Y. Liu, L. Jia, Q. Fang, and M. Yu, "Simultaneous implementation of XOR and XNOR operations using a directed logic circuit based on two microring resonators," *Opt. Express*, Vol. 19, No. 7, 6524, 2011.
9. Zhang, L., R. Ji, L. Jia, et al., "Demonstration of directed XOR/XNOR logic gates using two cascaded microring resonators," *Opt. Lett.*, Vol. 35, No. 10, 1620, 2010.